Grain Formation around the AGB Star L$_2$ Puppis Based On ALMA Observations

Joseph A. Nuth[1], Frank T. Ferguson[1,2], Ward Homan[3], Leen Decin[3] , and John A. Paquette[4]

[1] NASA-Goddard Space Flight Center 8801 Greenbelt Road, Greenbelt, MD 20071, USA; joseph.a.nuth@nasa.gov
[2] Catholic University of America 620 Michigan Avenue, Washington, DC 20064, USA
[3] Institute of Astronomy, KU Leuven Celestijnenlaan 200D B2401, B-3001 Leuven, Belgium
[4] Max-Planck Institute for Solar System Research Justus-von-Libieg-Weg 3 D-37077 Göttingen, Germany

Abstract

While models of grain formation in the outflows of carbon-rich stars have been relatively successful, models of outflows from oxygen-rich, asymptotic giant branch stars have been less fortunate. Under current modeling, it is difficult to produce sufficient amounts of silicate grains with high enough opacity to form a dust-driven wind from these stars. To investigate the cause of this difference, this work is a comparison between typical outflow model results and a model using input from Atacama Large Millimeter/submillimeter Array observations of L$_2$ Puppis. The temperatures from these observations are much lower than would typically be used in the standard outflow model. In addition, the observed gas densities are much higher than predicted from typical outflow models. Both of these differences make the formation of silicate grains much more favorable than predicted in current outflow models. We then explore the effects of other possible nonideal conditions including the efficiency of cluster growth prior to nucleation, the efficiency of grain growth following nucleation and the variation of grain coupling to stellar radiation during grain growth. Finally, we calculate the potential enhancement in grain production based on possible increased refractory abundances resulting from the vaporization of millimeter-scale and larger particles left over from the presence of a former planetary system.

Unified Astronomy Thesaurus concepts: Asymptotic giant branch stars (2100); Circumstellar dust (236); Circumstellar envelopes (237)

1. Introduction

Standard models of circumstellar outflows treat the shell as expanding into a vacuum with little or no interference from preexisting materials that may be in orbit around the star. However, exoplanets are no longer considered to be rare occurrences, but are found around almost every Sun-like star if we correct for observational selection effects (Batalha 2014; Ford 2014; Marcy et al. 2014). Planets range from Jupiter-sized objects orbiting much closer than Mercury orbits the Sun to Earth-sized planets spanning the range from much less than 1 au out to several au from the primary. Given this range of observed planets, there must also exist planetary debris such as asteroids and comets in most stellar systems, even if a small minority of systems fails to contain planets. Comets and asteroids in turn generate a steady-state dust population both near the ecliptic plane and extending well above and below this plane (Carrillo-Sánchez et al. 2016). We will compare a model using free expansion of the gas into vacuum with a model based on Atacama Large Millimeter/submillimeter Array (ALMA) observations of L$_2$ Puppis as a proxy for a stellar wind expanding into an existing solar system since L$_2$ Puppis is known to have a Jupiter-mass companion (Homan et al. 2017).

The exact details of the process leading to the Sun's asymptotic giant evolutionary phase may be somewhat uncertain, but the general scenario is quite well known. Once the Sun burns most of its hydrogen, it will swell and grow brighter. This will strip the atmospheres from the Earth and Venus, leaving bare, rocky crust exposed to the solar radiation and wind. Once the hydrogen in its core is exhausted, the Sun's outer envelope will swell to engulf Mercury and Venus, even though the lowered mass of the Sun will have caused these orbits to expand as well. Villaver and Livio have shown that planets within the stellar radius will spiral in and evaporate. In addition, for stars in the range of 1–5 $M_\odot$, planets with masses less than one Jupiter do not survive out to 3–5 au as the star leaves the asymptotic giant branch (AGB) stage and enters the planetary nebulae phase (Villaver & Livio 2007).

There have been studies on the enhancement of outflows from AGB stars perturbed by a large, Jupiter-sized companion. It is speculated that the gravitational attraction of the companion can pull material from the stellar surface, promoting mass loss from the star. Wang and Willson studied such an influence by modeling the dynamics of the orbital period of such a companion combined with the pulsation period of the AGB star. (Wang & Willson 2012) While they found the gravitational enhancement of the outflow to be small, they did find an interesting resonance in the system that resulted in a clustering of shocks with different speeds, resulting in spiral arms of higher gas density.

As an AGB star expands the result is the presence of significant reservoirs of refractory material orbiting within the stellar photosphere. For our own solar system, these reservoirs will include the remnants of Mercury, Venus, possibly the Earth and Moon, and maybe Mars. However, there are hundreds of thousands of smaller bodies distributed near the ecliptic plane that will also be affected. Of course, as noted above, not all stars will have a planetary system structured like our own. However, we can use our own solar system as a model for some simple calculations to explore the effects such refractory reservoirs might have on the winds observed around late stage stars.

Finally, most models of grain formation and growth assume that every collision between a gas-phase SiO molecule and a growing (SiO)$_x$ cluster or dust grain sticks with near unit efficiency. This is completely unrealistic for growing molecular-scale clusters where sticking coefficients based on

chemical kinetics could be many orders of magnitude less than 1. SiO additions to solid silica grains are also expected to be less efficient than unity. One of the first studies related to growth of solids from the vapor followed the growth of zinc crystals and demonstrated that for every 100,000 collisions of Zn atoms with a growing crystal, only three atoms actually stuck (Michael et al. 2003). Kimura et al. measured a similar sticking probability of only a few successful additions of Fe atoms to a growing Fe cluster for every 100,000 total collisions (Kimura et al. 2017).

Because freshly condensed silica dust is amorphous rather than crystalline it has many more potential sites available to incorporate gas-phase SiO molecules than would a crystalline grain and we therefore expect the sticking efficiency to be higher. We use our model to investigate the ultimate grain size, final wind outflow velocity, and fractional condensation of SiO into dust grains as a function of the SiO sticking coefficients to $(SiO)_x$ clusters and solids.

2. Contributions of "Solar System" Material to the Stellar Wind

If we simply assume that an asteroid or planet is engulfed by an expanding stellar photosphere and that, given sufficient time, its surface will come to equilibrium, then we can calculate the mass of vapor lost from its surface as a function of time. The dominant constituents in the crust and mantle of terrestrial planets are silicate minerals, primarily containing Mg and Fe. Magnesium has a much higher vapor pressure than either Fe or SiO while the vapor pressures of Fe and SiO are comparable. If we assume that the vapor pressure of the body is primarily controlled by the breakdown of silicate minerals and the loss of SiO rather than individual elemental vapor pressures, then we can use the vapor pressure equation from Ferguson & Nuth (2008) to calculate the SiO saturated vapor pressure, P_{sio}, as a function of temperature, T,

$$\log_{10}(P_{sio}/\text{Pa}) = 13.607\left(\frac{19{,}353}{T/(\text{K})}\right). \quad (1)$$

In this simple estimation, the body is assumed to behave similar to a growing/evaporating aerosol particle in the free-molecular pressure range. The change in the mass of this large particle, m_p, is given by

$$\frac{dm_p}{dt} = \frac{4\pi d_p^2\, V_{sio}(P - P_{sio})}{(2\pi m_{sio}kT)^{1/2}}, \quad (2)$$

where m_{sio} is the mass of a condensing SiO molecule, d_p is the diameter of the particle, V_{sio} is the volume of a condensing SiO molecule, t is time, P is the partial pressure of SiO, k is the Boltzmann constant, and T is the temperature of the grain (Friedlander 2000).

As the cosmic abundances of Fe, Mg, and Si are roughly equal, and excess O must also be present in these hot atmospheres along with minor elements such as Na, Ca, and Al, use of the SiO vapor pressure alone ensures that these vapor pressure calculations are a lower limit. Typical total densities at the edge of the photosphere range from 10^{-12} to 10^{-9} kg m^{-3} (Homan et al. 2017) and for most stars SiO is ∼one part in 10^6 by number when compared to H_2. So we can clearly ignore the partial pressure of SiO in the photosphere, P, in any calculation of the total mass loss rate from the equilibrated surface of a

silicate-based body engulfed by a stellar photosphere when using Equation (2). In addition, assuming a constant SiO density for the body, the mass loss expression given by Equation (2) can be changed to give the change in diameter, d_p, of the body with time:

$$\frac{d\,d_p}{dt} = \frac{-2V_{sio}P_{sio}}{(2\pi m_{sio}kT)^{1/2}}. \quad (3)$$

If the body is homogeneous, consists solely of SiO, and is held at a constant temperature, Equation (3) shows that the diameter of the body shrinks at a constant rate. A perfectly smooth Earth-sized body at 2000 K loses ∼0.5 cm s^{-1} while at 3000 K this increases to 712 cm s^{-1}. The diameter of the Earth is 1.29×10^9 cm and would evaporate in ∼78 yr at 2000 K or in less than 21 days at 3000 K. In either case, the SiO released would clearly overwhelm that contained in any stellar outflow. For a small body with a more realistic chemical composition, the vapor pressure of the equilibrated surface would be higher and the evaporation rate faster.

3. Evaporation under More Realistic Conditions

The previous calculations demonstrate that it is possible for the small bodies, moons, and planets around an AGB star to contribute significant quantities of refractory vapors (e.g., SiO) to a circumstellar outflow in excess of those usually assumed present in models of grain-driven winds (Gail & Sedlmayr 2013). There are a host of variables that can cause a decreased rate of planetary evaporation, the most important of which lead to nonequilibrium surface temperatures or much less efficient mass loss from the atmosphere of refractory vapor surrounding the evaporating body. As an example, a slowly rotating body surrounded by a partially transparent stellar envelope might radiate energy to space to maintain a lower surface temperature. A planetary-scale body will have significant thermal inertia, especially if the initial complement of radioactive elements was low and the planetary core has cooled and solidified. This thermal inertia would keep the surface cooler. As SiO and other materials vaporize, the latent heat of vaporization will also cool the surface.

The dynamics of planetary atmospheric loss are quite complicated and depend on the interaction of the stellar wind with the uppermost layers of the atmosphere. Other factors include the potential for active planetary magnetic fields (maybe the planet was initially enriched in long-half-life radioactive elements) that shield the exosphere from the stellar wind, or the possibility of remnant magnetic fields that could partially shield the surface. However, for SiO densities typical of AGB outflows (10^{-16}–10^{-13} kg m^{-3}) even a slow leak from the planets SiO-rich atmosphere into the AGB photosphere could easily increase the concentration of condensable SiO molecules by several orders of magnitude. For much smaller bodies and for dust grains near the ecliptic plane, vaporization could be nearly instantaneous. Evaporation from bodies in an ecliptic plane would create a preferred orientation for mass loss leading to the observation of disks and discontinuities in the chemistry of the outflow (Homan et al. 2017).

In summary, if our own solar system is used as a model for the mass distribution around a typical low mass AGB star, then a wide range of refractory sources are available to feed condensable materials into the wind. Micron-sized dust is produced continuously from asteroids and comets and this

evaporates instantly as these particles are engulfed by the stellar photosphere or fall into and enrich the photosphere due to Poynting–Robertson or gas drag (Weidenschilling 1977, 2006). Asteroids (and comets) evaporate over longer timescales depending on their initial size and distance from the star. The evaporation of terrestrial-sized planets is a much more complicated and long term process that could potentially supply SiO to the wind for the life of the outflow while the "evaporation" of gas giants could significantly affect the local gas-phase chemistry of the wind by supplying reduced carbon and nitrogen compounds from the atmosphere into the wind (Homan et al. 2018).

4. Description of a Simple Standard Model

In this section, the stellar outflow is modeled as a spherically symmetric, steady system. The model closely follows that described in an earlier work and this work may be consulted for further details (Paquette et al. 2011). In this earlier work, the steady-state continuity and momentum equations for the system were combined into a single wind equation for the outflow velocity. In the current work, these equations are solved individually in their transient form:

$$\frac{\partial \rho}{\partial t} + \frac{1}{r^2}\frac{\partial}{\partial r}(\rho r^2 v) = 0 \qquad (4)$$

$$\frac{\partial \rho v}{\partial t} + \frac{1}{r^2}\frac{\partial}{\partial r}(\rho r^2 v^2) = -\frac{\partial p}{\partial r} - \frac{\rho G M_\star (1-f)}{r^2}, \qquad (5)$$

where ρ is the gas density, v is the outflow velocity, p is the gas pressure, r is the radial coordinate, G is the universal gravitational constant, $M_\star$ is the stellar mass, and the factor f is the ratio of the radiative pressure on the grains to the gravitational force given by

$$f = \frac{N_g a^2 \overline{Q_{pr}} L_\star}{4cGM_\star \rho_g}, \qquad (6)$$

where N_g is the number density of grains of radius, a, c is the speed of light, $L_\star$ is the stellar luminosity, and ρ_g is the grain density. The efficiency factor for radiation pressure, Q_{pr}, is a function of the index of refraction for the grain, m, the wavelength of light, λ, and the grain radius, a. The average efficiency factor for radiation pressure, $\overline{Q_{pr}}$, is calculated with

$$\overline{Q_{pr}} = \frac{\int_0^\infty Q_{pr}(m, \lambda, a) B_\lambda(T, \lambda)d\lambda}{\int_0^\infty B_\lambda(T, \lambda)d\lambda} \qquad (7)$$

assuming that the stellar radiation is given by the Planck blackbody function, $B(\lambda, T)$, at the temperature of the star, $T_\star$. Values of Q_{pr} are calculated via Mie theory using the optical properties of the astronomical silicate (Draine & Lee 1984).

At present, the only condensible species considered in the outflow is silicon monoxide. Vapor pressure data for SiO are taken from recently updated measurements (Nuth & Ferguson 2006; Ferguson & Nuth 2008). As the outflow leaves the star, the mass fraction of SiO, w_{SiO}, will decrease by both the nucleation and growth of grains. These losses combined with the transport equation for the SiO mass fraction are given by

$$\frac{\partial \rho w_{sio}}{\partial t} + \frac{1}{r^2}\frac{\partial(\rho r^2 v\, w_{sio})}{\partial r} = -Jv^* \rho_{sio} - N_g \cdot \frac{dm_p}{dt}, \qquad (8)$$

where J is the nucleation rate of critical clusters of volume v^*, both calculated via Classical Nucleation Theory. These clusters are assumed to have a density of ρ_{sio}. N_g is the number density of grains and the change in the particle mass, m_p, and density ρ_{sio}. The particle growth rate is taken from Equation (2) for the free-molecular regime (Friedlander 2000):

$$\frac{dm_p}{dt} = \alpha_g \times \frac{4\pi d_p^2 V_{sio}(P - P_{sio})}{(2\pi m_{SiO}kT)^{1/2}}. \qquad (9)$$

In this case, Equation (9) differs from Equation (2) by the term, α_g, which is a factor that accounts for the fraction of collisions that result in grain growth. While an $\alpha_g \sim 1$ would mean that every collision was successful in condensing into the growing grain, previous studies on grain growth have indicated that this factor can often be much smaller (Michael et al. 2003; Kimura et al. 2017).

The nucleation rate, J, is calculated using the Classical Nucleation expression

$$J = \alpha_j \times n_1^2 V_{sio}\left(\frac{2\sigma}{\pi m_{sio}}\right)^{1/2} \exp\left[\frac{-16\pi\sigma^3 V_{sio}^2}{3(kT)^3 \ln^2(S)}\right], \qquad (10)$$

where n_1 is the monomer number density, V_{sio} is the volume of an SiO molecule, and σ is the surface tension. The supersaturation ratio, S, is the ratio of the partial pressure of SiO to its equilibrium vapor pressure. As in the growth rate case, an efficiency term, α_j, is added to this expression to account for ineffective SiO cluster growth collisions that are below this theoretical maximum. In a previous paper (Donn & Nuth 1985) it was argued that Nucleation Theory was not applicable to conditions in circumstellar outflows because the precondensation cluster distributions of SiO would be considerably less abundant than expected in an equilibrated gas. However, later work (Paquette & Nuth 2011) has shown that the extreme sensitivity of Classical Nucleation Theory to changes in temperature and supersaturation can compensate for reductions in the concentration of critical clusters in the gas by as much as four orders of magnitude.

In previous work, a set of three moment equations were used to track the grain population (Paquette et al. 2011). These three moments allowed the calculation of the grain number density, the mean grain radius, and the width of the particle size distribution. In this work, a simpler model of the grain population is used where the grains are considered to be monodisperse. Therefore, instead of three moment equations as used before only two equations are used to give particle size and number density. Two quantities, M_0 and M_1, are defined per unit mass of the gas and are used to track the size and number of grains. The first term, M_0, is defined as the number of grains per unit mass of the gas. Therefore, the total number of grains per unit volume, N_g, and M_0 are related via:

$$N_g = \rho M_0, \qquad (11)$$

where ρ is the local gas density. The change in the total number of grains is given by the nucleation of new grains via the nucleation rate, J, as

$$\frac{\partial(\rho M_0)}{\partial t} + \frac{1}{r^2}\frac{\partial(\rho r^2 v\, M_0)}{\partial r} = -J. \qquad (12)$$

The second quantity, M_1, is defined as the mass of solid in the grains per unit mass of the gas. While w_{sio} represents the amount of gaseous SiO per unit mass of gas, M_1 gives the amount of condensed SiO per unit of gas. The equation for M_1 is therefore very similar to the SiO mass fraction equation, but in this case the loss terms become source terms as particles nucleate and grow. The equation for M_1 is

$$\frac{\partial(\rho M_1)}{\partial t} + \frac{1}{r^2}\frac{\partial(\rho r^2 v\, M_1)}{\partial r} = Jv^*\rho_{sio} + N_g \cdot \frac{dm_p}{dt}. \quad (13)$$

Knowing the total amount of condensed SiO and the total number of particles, the particle size can be calculated assuming the grains are spherical with a density similar to the bulk density of SiO.

In the current model, the envelope is also assumed to be optically thin with frequency-independent opacity so that the temperature field can be assumed to follow a $r^{-1/2}$ dependency on distance from the star (Paquette et al. 2011)

$$T(r) = T_*\left(\frac{R_*}{r}\right)^{1/2}, \quad (14)$$

where T_* is the temperature of the star of radius R_*. For calculation of the outflow, the gas is assumed to behave ideally with a molecular weight of 1.28 g/g-mole.

For a given set of stellar parameters, stellar radius, $R_\star$, temperature, $T_\star$, stellar mass, $M_\star$, and initial gaseous SiO abundance, the above equations are solved for the SiO mass fraction, outflow velocity, and grain concentration. The total gas density and SiO mass fraction are set at the photosphere of the star while the velocity and grain number density functions are set to zero. At a sufficiently far distance, the outflow reaches a terminal velocity where there is no gradient in these values.

5. L$_2$ Puppis Observations

L$_2$ Puppis is a semi-regular, pulsating variable with a period of 141 days and a mass of 0.659 $M_\odot$. Based on its spectral type it has an estimated effective temperature of ~3500 K. L$_2$ Puppis has a compact dust disk around the star with an inner rim starting at approximately 6 au and an outer edge at 13 au. Using a combination of ALMA observations of the ^{12}CO $J = 3 - 2$ and ^{13}CO $J = 3 - 2$ rotational transitions and 3D radiative transfer modeling, Homan et al. were able to deduce the temperature and density around the central star (Homan et al. 2017).

The computed temperatures from Homan et al. are shown in Figure 1 and the temperature profile is characterized over three different sections. In the first section (<6 au), there is a steep drop in temperature down to ~500 K. This region, starting at approximately 6 au, represents the inner edge of the dust disk as determined by Kervella et al. (2015). In the region 6–13 au, corresponding to the dust disk, there is a plateau in the temperature at ~500 K. In the third region beyond this dust disk there is a further, steep drop to very cold temperatures (~100 K). Homan et al. provided an analytical fit to the temperature profile as well as a fit based on several, power-law sections. This temperature profile along with these power-law segments are plotted in Figure 1. From the temperature measurements, the effective temperature of 3500 K gives a stellar radius, $R_* = 1.02$ au. Using these values in Equation (14) yields the linear profile shown in Figure 1. The first power-law
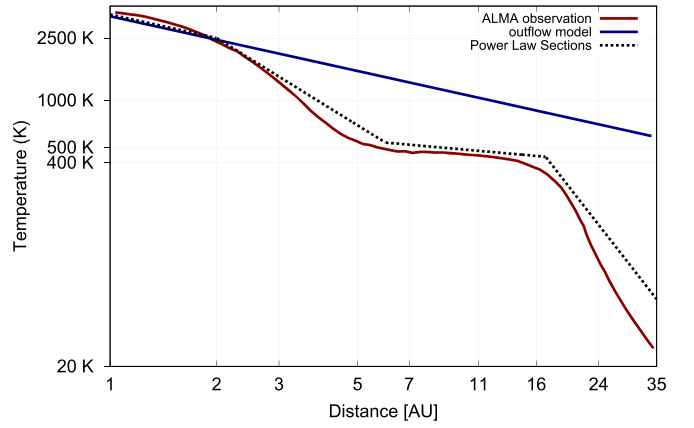

Figure 1. Temperature profiles of L$_2$ Puppis. Shown in the figure are the results from ALMA observation (red curve), power-law sections that approximate this curve (black dashed curve), and approximation assuming an optically thin envelope (blue curve).
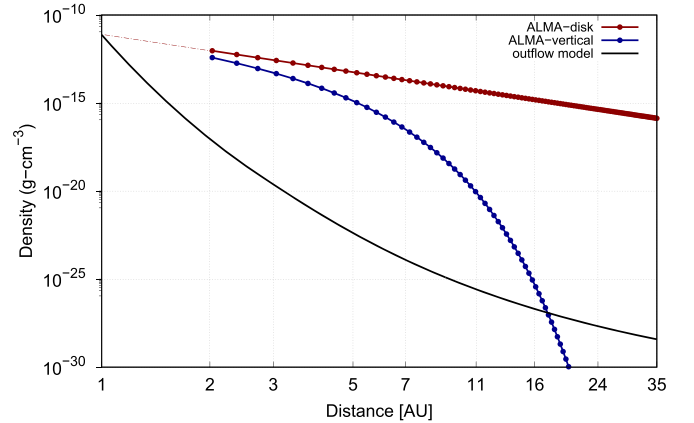

Figure 2. Comparison of density profiles for L$_2$ Puppis. Shown in the figure are the density profile along the horizontal, disk plane (red curve), the vertical density profile (blue curve), and the hydrostatic density profile calculated from the outflow model (black curve).

expression given by Homan et al. for $r < 2$ au also has an exponent of -0.5; therefore Equation (14) and the power-law section agree in this first zone for temperatures above ~2500 K. Beyond this point, the results from Homan et al. fall far below the optically thin approximation of a standard outflow model. This is especially significant for grain formation since grains are expected to first nucleate at ~1000 K. Using Equation (14), 1000 K is not reached until approximately 11 au, well beyond the inner region of the dust disk at approximately 6 au. In contrast, the results from Homan et al. show that 1000 K occurs at approximately 4 au. Using the lower values of the temperature from Homan et al. definitely increases the feasibility for grain formation in the outflow.

Homan et al. also provided density profiles in the $r - z$ plane for L$_2$ Puppis for $r > 2$ au. Along the plane of the disk, the density follows a simple power-law drop with an exponent of -3.1 and is shown as the red line in Figure 2. For any height above the disk plane the drop in density is steeper. The vertical density profile above the star is also shown as the blue line in Figure 2. To make a comparison between the standard outflow model and the density from the ALMA observations, the density at the photosphere near 1 au needs to be estimated. In this case, the density is extrapolated back to this point using the expression given by the ALMA disk expression as shown by
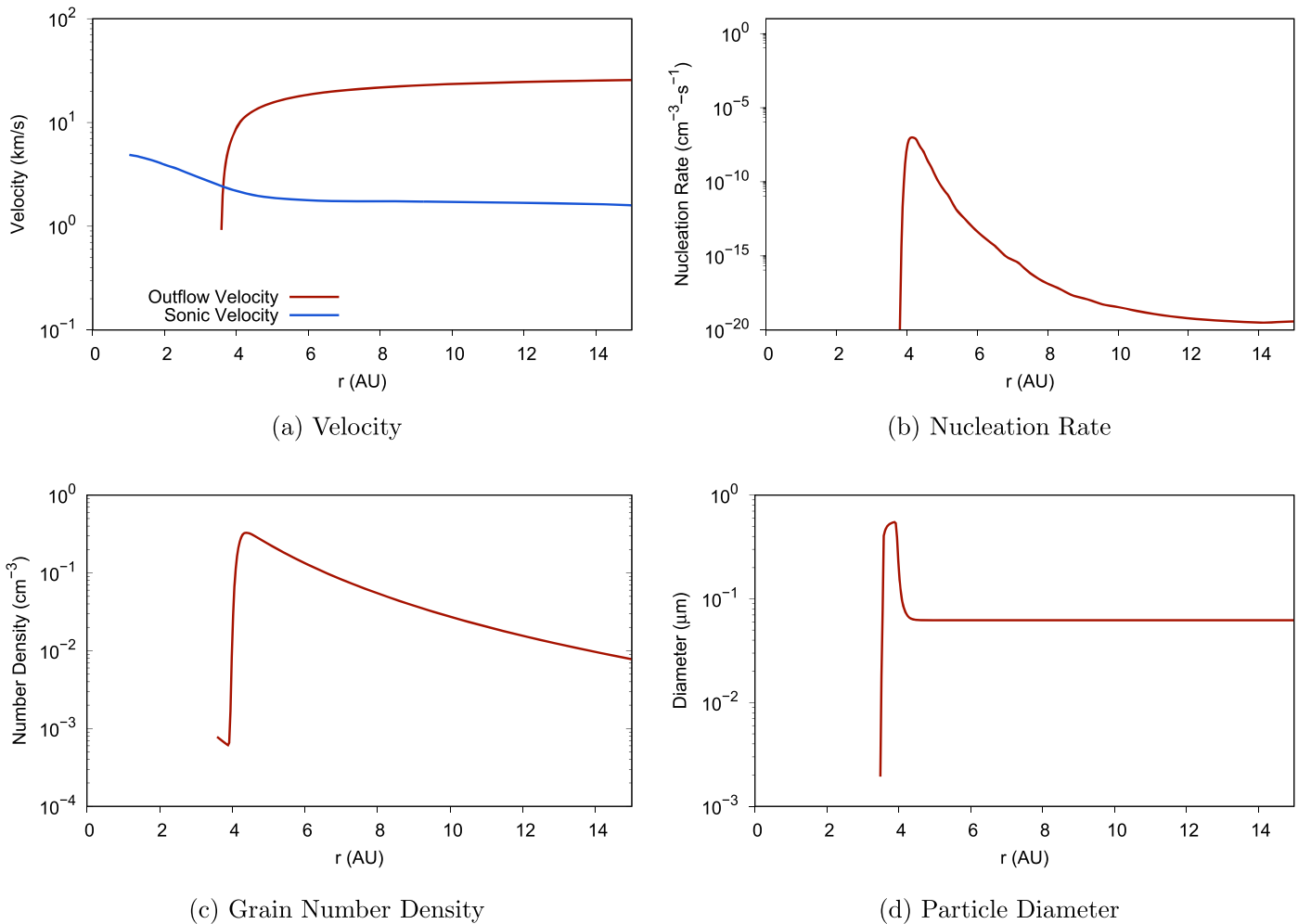
(a) Velocity

(b) Nucleation Rate

(c) Grain Number Density

(d) Particle Diameter

Figure 3. Outflow calculation using the temperature and density profile for L_2 Puppis from Homan et al. Shown in the figure are the calculated (a) outflow velocity and sonic velocity, (b) the SiO nucleation rate, (c) the number density of SiO grains, and (d) the diameter of the grains.
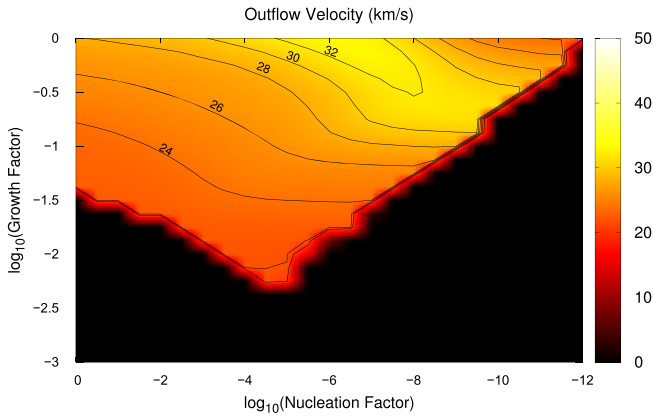
the dashed red line in the figure. The density calculated using the model outlined in Section 4 is shown as the black line in Figure 2. In this case, the density at the photosphere is set equal to the extrapolated value at ~1 au and corresponds to a hydrostatic density profile. As shown in the figure, both the horizontal and vertical density profiles from L_2 Puppis are larger than this density profile out farther than the outer edge of the dust disk at ~13 au. In addition, the density profile along the disk is many orders of magnitude greater than this hydrostatic density field. These higher observed densities also make the formation of grains more favorable compared to the standard outflow model.

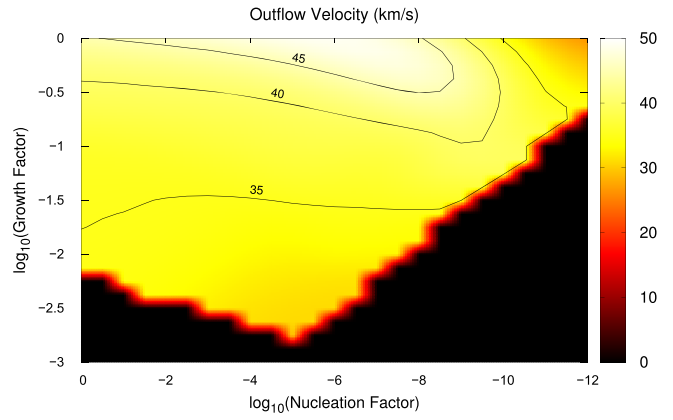## 6. Outflow Model Results Using L_2 Puppis Observations

Using the values of the stellar parameters for L_2 Puppis, the equations listed in Section 4 can be solved for the SiO mass fraction, outflow velocity, and grain concentration profiles. Specifically, these values are $T_* = 3500$ K, $M_* = 0.659\,M_\odot$, and $R_* = 1.02$ au. Based on solar abundances, the mass fraction of SiO in the gas was estimated as 1.16×10^{-3}. When these values were input to the standard outflow model, no grains were formed. The gas temperatures were too high and the gas densities were too low for the SiO to nucleate and for grains to grow.

The next step was to use the information from Homan et al. as input to the outflow model. Rather than calculate the temperature and density profile using Equations (4) and (14), these values were taken directly from the results of Homan et al. In this case, grains did form and a dust-driven wind occurs. A summary of these results is shown in Figure 3.
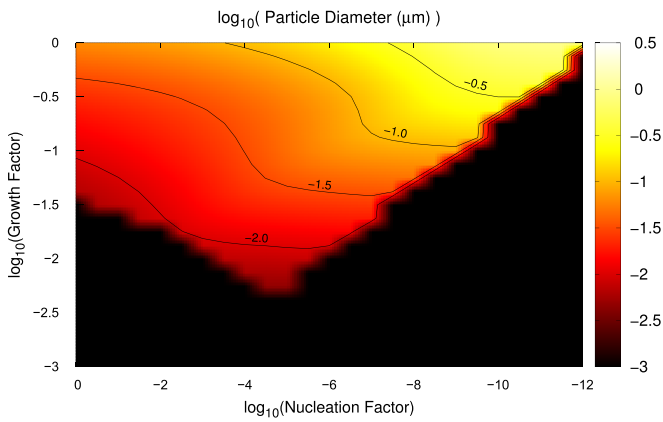
Figure 3 shows the computed results for (a) the outflow velocity, (b) the grain nucleation rate, (c) the grain number density, and (d) the grain diameter. As shown in Figure 3(b), grain nucleation occurs at ~4 au. The resulting grains drive the gas past the sonic point, which is at 4 au. Final calculated grain diameters are approximately 0.06 μm. It is interesting to note that the initial nucleation of grains takes place just before the observed location of the inner edge of the dust disk at 6 au. In the current modeling, grains are considered to be monodisperse and the distribution of grain sizes at any one point is not considered. The particle size that we report is an instantaneous result computed at any particular stellar radius by converting the condensed mass into a monodispersed number of particles. When particles first nucleate they quickly grow in size but because of the tail in the nucleation rate curve of Figure 3(b), smaller particles continue to be generated and reduce the overall particle size. The result is a sharp maximum in the particle diameter as shown in Figure 3(d) which later drops to a smaller grain size.
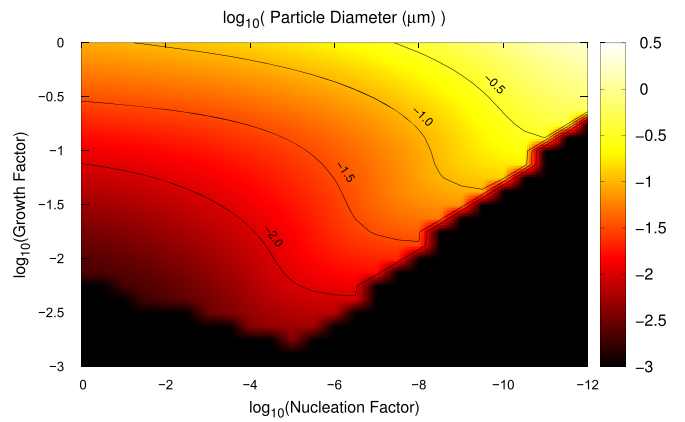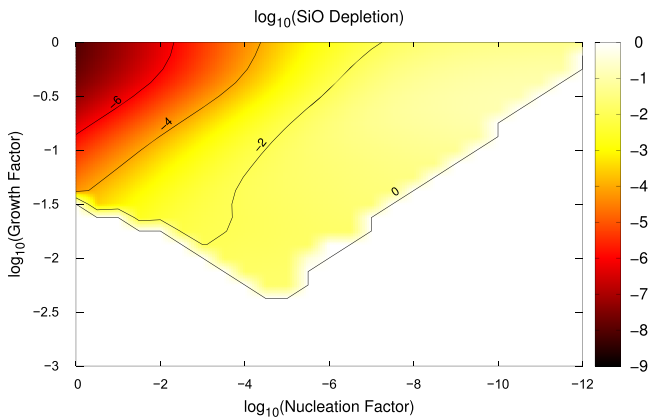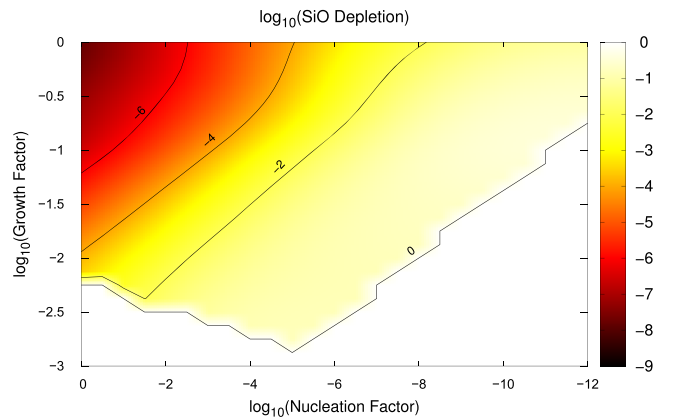
(a)

(b)

(c)

Figure 4. Contour map of outflow solutions for different values of growth and nucleation factors and a mass fraction of SiO of 1.16×10^{-3}. Shown in the figure are the (a) terminal velocities of the dust-driven wind if it exists, (b) the resulting grain diameters in microns, and (c) the fraction of the remaining SiO in the gas stream compared to the initial amount.

(a)

(b)

(c)

Figure 5. Contour map of outflow solutions for different values of growth and nucleation factors and a mass fraction of SiO of 2.32×10^{-3}. Shown in the figure are the (a) terminal velocities of the dust-driven wind if it exists, (b) the resulting grain diameters in microns, and (c) the fraction of the remaining SiO in the gas stream compared to the initial amount.

The outflow calculations shown in Figure 3 are made assuming idealized growth and nucleation; i.e., that every collision results in successful growth. In other words, the factors, α_g, in Equation (9) and, α_j, in Equation (10) have both

been set to 1. To investigate the range in these parameters in which a dust-driven wind was still possible, an array of outflow calculations were made with various values of these factors. The value of the nucleation factor, α_j, was varied from 10^{-12} to

1.0 while the growth factor, α_g, was varied from 10^{-3} to 1.0. The results of these calculations are shown in Figure 4.

Figure 4(a) is a plot of the terminal velocity of the outflow as a function of these growth and nucleation factors. As shown in the figure there is a sharp transition between the regions where a dust-driven wind exists and those where such a wind does not exist. For those solutions where a dust-driven wind exists, the outflow velocities range from $\sim$20 to 35 km s^{-1}. Interestingly, for a high growth factor, it is still possible to have a dust-driven wind even with nucleation rate factors as low as $\sim 10^{-11}$. This is consistent with the non-LTE results obtained by Paquette & Nuth (2011). For intermediate values of the nucleation factor (e.g., 10^{-4}–10^{-5}), a dust-driven wind exists for growth factors as low as $\sim$0.005.

Plotted in Figure 4(b) is the resulting final diameter of the grains formed in the dust-driven wind. Particle sizes for a dust-driven wind range from $\sim$0.005 to 1.0 μm. As could be expected, the largest particles occur at conditions where the nucleation rate is the lowest and growth factors are at a maximum. For any given growth factor, the final size of the grains is higher for grains with lower nucleation factors, consistent with fewer grains being formed and allowed to grow to larger sizes in a supersaturated environment.

Finally, Figure 4(c) is a plot of the ratio of the SiO gas in the final outflow to the initial starting amount. At the highest nucleation and growth factors, the SiO vapor is severely depleted due to the nucleation and growth of grains with a drop of $\sim$9 orders of magnitude. For most of the cases in which grains form, the mass fraction of SiO in the vapor drops by $\sim$2 orders of magnitude.

7. L$_2$ Puppis Results Including Possible Solar System Debris

As noted above, nearly all stars have planets, and a planetary-scale companion has been observed in the disk of L$_2$ Puppis (Homan et al. 2017). If we use our solar system as a model, the presence of a Jupiter-sized planet could imply the presence of at least a debris disk consisting of asteroids and dust as well as a population of comets and additional dust both above and below the ecliptic plane. An increase in the stellar wind will generate drag on larger dust grains as will increased stellar luminosity. Both effects will cause dust to spiral inward until the dust grains eventually cross the dust evaporation front and thus add SiO molecules to the expanding wind. In this section, we will investigate the effects on the outflow of a refractory-enriched wind.

Figure 5 is similar to Figure 4, plotting the terminal outflow velocity, grain size, and gas-phase SiO abundance ratio compared to the initial abundance as a function of the nucleation and grain growth factors, but with an initial SiO abundance in the disk that is enriched by a factor of two over cosmic abundances. This assumes that preexisting dust grains have migrated inward, evaporated, and been incorporated into the gas flow inside 2–3 au, e.g., prior to the conditions where dust condensation and growth occur. As can be seen by comparison of Figures 4 and 5, at any point in (Growth Factor) versus (Nucleation Factor) space, the resulting terminal outflow velocity, particle diameter, and SiO depletion fraction in the disk increase as might be expected from the addition of more condensable material in the outflowing gas.

A solar system is not spherically symmetric and neither is the density distribution observed around L$_2$ Puppis and shown in
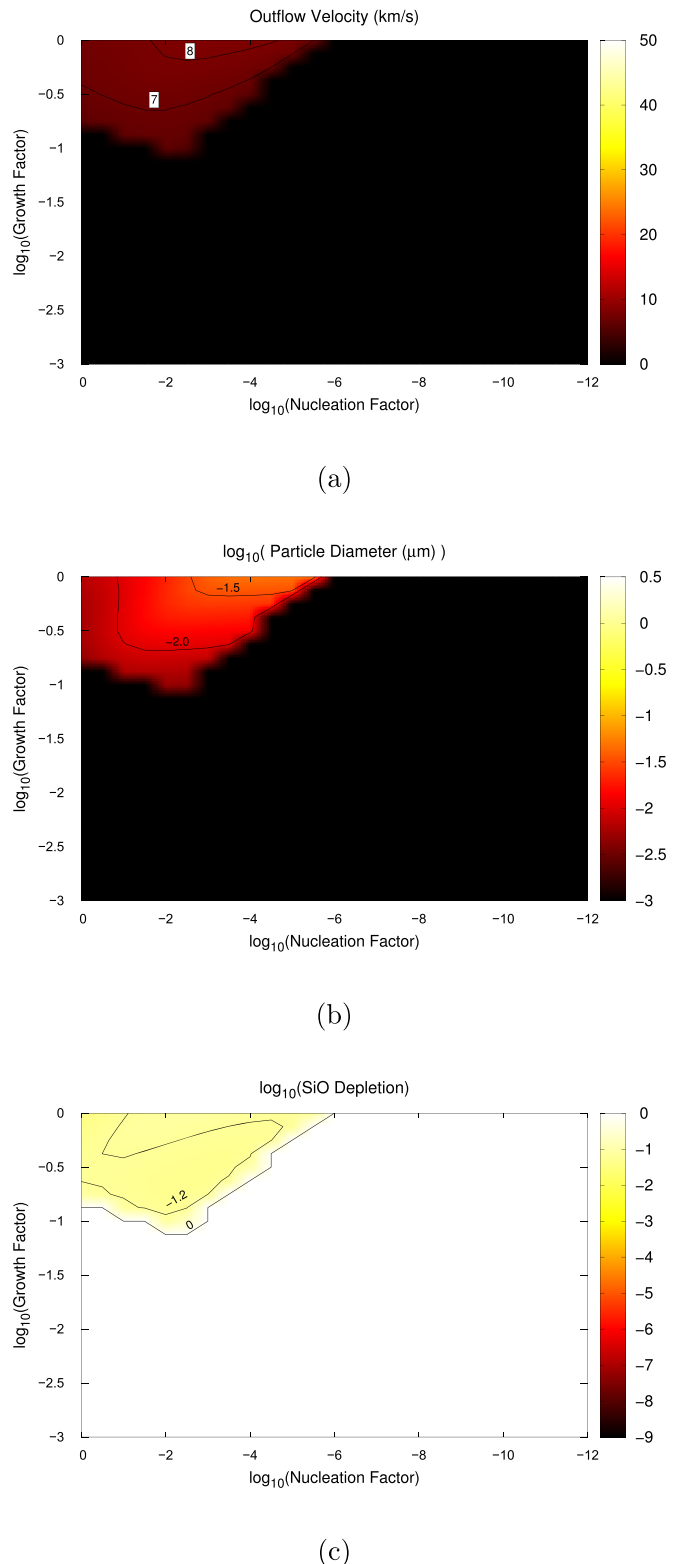

(a)

(b)

(c)

Figure 6. Contour map of outflow solutions for different values of growth and nucleation factors and a mass fraction of SiO of 1.16×10^{-3} using the vertical density profile of L$_2$ Puppis. Shown in the figure are the (a) terminal velocities of the dust-driven wind if it exists, (b) the resulting grain diameters in microns, and (c) the fraction of the remaining SiO in the gas stream compared to the initial amount.

Figure 2. We therefore performed outflow calculations using the density profile along the polar vector based on the blue curve in Figure 2. The results are displayed in Figure 6, again

showing the terminal outflow velocity, grain size, and gas-phase SiO abundance ratio compared to the initial abundance as a function of the nucleation and grain growth factors, assuming normal cosmic abundances. Under these circumstances, grain formation, terminal outflow velocities, and particle diameters for any point in (Growth Factor) versus (Nucleation Factor) space are greatly reduced and thus the stellar wind is far from spherical symmetry.

Figure 7 is similar to Figure 6, plotting the terminal outflow velocity, grain size, and gas-phase SiO abundance ratio compared to the initial abundance as a function of the cluster and grain growth efficiencies, but with an initial SiO abundance in the disk that is enriched by a factor of 10 over cosmic abundances. This enrichment increases the range in (Growth Factor) versus (Nucleation Factor) space that produces dust grains and leads to a significant increase in the potential terminal wind velocity and grain size.
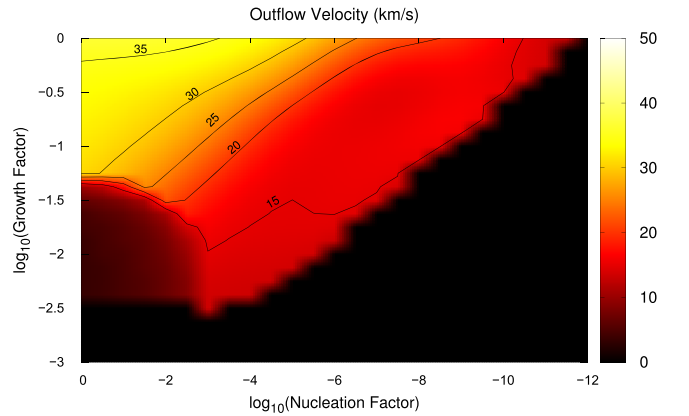
8. Discussion

The results in Figures 4–7 are in (Growth Factor) versus (Nucleation Factor) space and both of these efficiency factors are expected to be nearly single-valued with some distribution around the mean due to the effects of temperature, pressure, and possibly gas composition. Unfortunately, we have no experimental evidence that directly measures these quantities for the condensation of SiO from the gas phase. Based on chemical kinetic considerations and the measurements of Michael et al. we can assume that both factors are less than unity—and possibly much less than unity. (Michael et al. 2003; Kimura et al. 2017) Only one point in each of these diagrams represents reality. While it is clear that nucleation and grain growth are an important consideration in models of grain growth in circumstellar outflows, better models must await measurement of these factors.
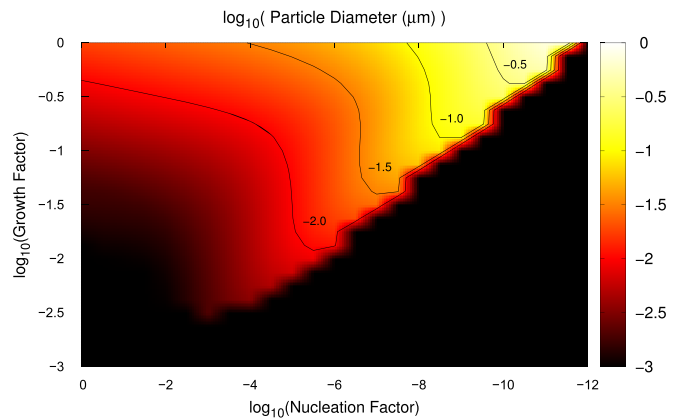
Another result of these models is the importance of preexisting refractory material around a dying star and its potential contribution to the properties of a stellar outflow. Not only can such material contribute significantly to the condensable vapor in any specific direction, but the enhanced winds can drive significant asymmetries in the outflow itself depending on the distribution of the preexisting material. A caveat in our results is our use of the optical properties of astronomical silicate (Draine & Lee 1984) to calculate the photon pressure on newly condensed dust grains. It is certainly possible that very fresh dust particles have optical properties significantly different from dust that has been annealed in the high temperature outflow (e.g., Hallenbeck et al. 2000), or irradiated in the interstellar medium. For our purposes, although the absolute value of the terminal wind velocity may be less than the numbers calculated in Figures 4–7 depending on the actual optical properties of freshly condensed dust, the relative trends should be correct.
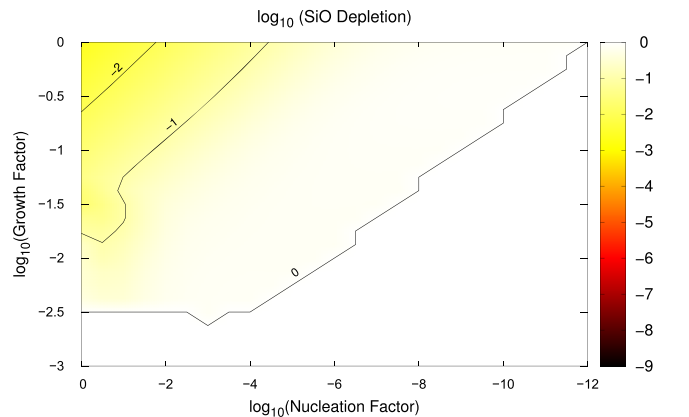
9. Conclusions

Our results have demonstrated that chemical factors such as the nucleation efficiency and the SiO-grain growth efficiency can have very large effects on the dust nucleation rate, the grain size distribution, and the final gas outflow velocity for winds around AGB stars. At the present time the values of these factors are largely unknown, but are at least several orders of magnitude smaller than the typically assumed value of unity

(a)

(b)

(c)

Figure 7. Contour map of outflow solutions for different values of growth and nucleation factors and a mass fraction of SiO of 1.16×10^{-2} using the vertical density profile of L_2 Puppis. Shown in the figure are the (a) terminal velocities of the dust-driven wind if it exists, (b) the resulting grain diameters in microns, and (c) the fraction of the remaining SiO in the gas stream compared to the initial amount.

(e.g., every SiO collision with a growing $[SiO]_x$ cluster does NOT stick). Similarly, the efficiency of grain growth from refractory vapors is also likely to be low. The first factor

hinders the formation of grain nuclei in an outflow while the second factor hinders grain growth. Paquette & Nuth (2011) demonstrated that decreasing the number of stable grain nuclei simply shifts the point of maximum grain formation to slightly larger stellar radii (Paquette & Nuth 2011). However, decreasing the efficiency of grain growth could result in a smaller average grain size and a more efficient coupling of the dust to the stellar radiation field per unit of SiO in the outflow. This speculation will depend on the optical properties of small, freshly formed dust grains that may be highly disordered and very different from the properties of astronomical silicate.

Finally, the practice of assuming that stellar outflows are simple hydrodynamic expansions of gas into the relative vacuum of the interstellar medium is no longer valid. Observational evidence shows that most stars have planets and this implies the presence of additional refractory solids such as moons, asteroids, and smaller dust grains. As they evaporate such materials will provide the hot, expanding photospheric gas with additional refractory vapors including especially SiO, Fe, and Mg that will aid both grain nucleation and dust growth. The planar nature of planetary systems will lead to the preferential formation of dust grains along the ecliptic plane due to the higher concentrations of refractory vapors in the winds flowing past evaporating silicate bodies. Trails of cometary debris could form linear reservoirs above and below the ecliptic plane. All of these refractory reservoirs will, in turn, lead to significant asymmetries both in the outflows and in the resultant planetary nebulae.

ORCID iDs

Leen Decin ● https://orcid.org/0000-0002-5342-8612
John A. Paquette ● https://orcid.org/0000-0003-1155-3068

References

Batalha, N. M. 2014, PNAS, 111, 12647
Carrillo-Sánchez, J. D., Nesvorný, D., Pokorný, P., Janches, D., & Plane, J. M. C. 2016, GeoRL, 43, 11979
Donn, B., & Nuth, J. A. 1985, ApJ, 288, 187
Draine, B. T., & Lee, H. M. 1984, ApJ, 285, 89
Ferguson, F. T., & Nuth, J. A. 2008, Journal of Chemical Engineering Data, 53, 2824
Ford, E. B. 2014, PNAS, 111, 12616
Friedlander, S. K. 2000, Smoke, Dust, and Haze: Fundamentals of Aerosol Dynamics (New York: Oxford Univ. Press)
Gail, H.-P., & Sedlmayr, E. 2013, Physics and Chemistry of Circumstellar Dust Shells, Cambridge Astrophysics (Cambridge: Cambridge Univ. Press), doi:10.1017/CBO9780511985607
Hallenbeck, S. L., Nuth, J. A. I., & Nelson, R. N. 2000, ApJ, 535, 247
Homan, W., Danilovich, T., Decin, L., et al. 2018, A&A, 614, A113
Homan, W., Richards, A., Decin, L., et al. 2017, A&A, 601, A5
Kervella, P., Montargès, M., Lagadec, E., et al. 2015, A&A, 578, A77
Kimura, Y., Tanaka, K. K., Nozawa, T., Takeuchi, S., & Inatomi, Y. 2017, SciA, 3, e1601992
Marcy, G. W., Weiss, L. M., Petigura, E. A., et al. 2014, PNAS, 111, 12655
Michael, B. P., III, J. A. N., & Lilleleht, L. U. 2003, ApJ, 590, 579
Nuth, J. A. I., & Ferguson, F. T. 2006, ApJ, 649, 1178
Paquette, J. A., Ferguson, F. T., & Nuth, J. A. 2011, ApJ, 732, 62
Paquette, J. A., & Nuth, J. A. 2011, ApJL, 737, L6
Villaver, E., & Livio, M. 2007, ApJ, 661, 1192
Wang, Q., & Willson, L. A. 2012, ApJ, 755, 136
Weidenschilling, S. J. 1977, MNRAS, 180, 57
Weidenschilling, S. J. 2006, Icar, 181, 572